Taura syndrome virus IRES initiates translation by binding its tRNA-mRNA–like structural element in the ribosomal decoding center

Cha San Koh[a,1], Axel F. Brilot[b,1], Nikolaus Grigorieff[b,c,2], and Andrei A. Korostelev[a,2]

[a]RNA Therapeutics Institute, Department of Biochemistry and Molecular Pharmacology, University of Massachusetts Medical School, Worcester, MA 01605; [b]Department of Biochemistry, Brandeis University, Waltham, MA 02454; and [c]Howard Hughes Medical Institute, Janelia Farm Research Campus, Ashburn, VA 20147

Edited* by Jennifer A. Doudna, University of California, Berkeley, CA, and approved May 13, 2014 (received for review April 6, 2014)

In cap-dependent translation initiation, the open reading frame (ORF) of mRNA is established by the placement of the AUG start codon and initiator tRNA in the ribosomal peptidyl (P) site. Internal ribosome entry sites (IRESs) promote translation of mRNAs in a cap-independent manner. We report two structures of the ribosome-bound Taura syndrome virus (TSV) IRES belonging to the family of Dicistroviridae intergenic IRESs. Intersubunit rotational states differ in these structures, suggesting that ribosome dynamics play a role in IRES translocation. Pseudoknot I of the IRES occupies the ribosomal decoding center at the aminoacyl (A) site in a manner resembling that of the tRNA anticodon-mRNA codon. The structures reveal that the TSV IRES initiates translation by a previously unseen mechanism, which is conceptually distinct from initiator tRNA-dependent mechanisms. Specifically, the ORF of the IRES-driven mRNA is established by the placement of the preceding tRNA-mRNA–like structure in the A site, whereas the 40S P site remains unoccupied during this initial step.

tRNA-mRNA mimicry | IRES-dependent initiation | factor-independent initiation | FREALIGN | real-space refinement

Protein synthesis relies on precise placement of the ORF within the ribosome during translation initiation. Canonical initiation in eukaryotes depends on a 7-methylguanosine cap at the 5′ terminus of mRNA and on extraribosomal initiation factors (1). Following a stepwise assembly, the 80S initiation complex contains the initiator methionyl-tRNA^{Met} and the AUG start codon in the peptidyl (P) site. Some viral mRNAs use alternative cap-independent mechanisms that involve internal ribosome entry sites (IRESs) (2). IRESs are folded RNA structures in the 5′ UTR that promote formation of the 80S initiation complex in the presence of fewer initiation factors than required for cap-dependent initiation (3).

The ribosomal P-site employment in initiation is thought to be ubiquitous for cap-dependent and IRES-dependent translation (4). Of the four groups of known IRESs, the most streamlined mechanism has been described for IRESs from the Dicistroviridae family of arthropod-infecting viruses. The Dicistroviridae genome has two ORFs separated by an intergenic region (IGR). The IGR contains an IRES that drives translation of the second ORF without the aid of initiation factors (4). Based on phylogenetic analyses of the structural polyprotein ORF2 and IGR IRES, the Dicistroviridae viruses are divided into the genus *Cripavirus* [including cricket paralysis virus (CrPV), Drosophila C virus, and *Plautia stali* intestine virus (PSIV)] and *Aparavirus* [including Taura syndrome virus (TSV), Kashmir bee virus, and acute bee paralysis virus] (4). Biochemical studies suggest that despite differences between some secondary structure elements of *Cripavirus* and *Aparavirus* IRESs, the molecular mechanisms of translation initiation are similar (5). IGR IRESs can initiate translation on ribosomes from yeast, wheat, human, and other eukaryotic organisms, indicating that the molecular mechanism of IGR IRES-driven initiation in eukaryotes is conserved and is not species-specific (6–10).

In contrast to cap-dependent initiation and initiation from other groups of IRESs, translation from IGR IRESs starts from a non-AUG start codon and does not involve initiator methionyl-tRNA^{Met}. Translation from the majority of IGR IRESs, including the CrPV and TSV IRESs, initiates with alanyl-tRNA^{Ala} (7, 9, 10). IGR IRESs contain three pseudoknots. At the 5′ region, pseudoknot II (PKII) and PKIII, which are critical for formation of the 40S•IRES and 80S•IRES complexes (8, 9), form a double-nested pseudoknot (11, 12). PKI, located immediately upstream of the start codon, forms a separate domain at the 3′ region of the IRES. This domain is essential for the function of IGR IRESs (13). The crystal structure of an isolated PKI of the CrPV IGR IRES shows that the pseudoknot resembles the anticodon stem loop of tRNA bound to a cognate mRNA codon (14, 15). Isolated PKI of CrPV and PSIV IRESs binds to the P site of the bacterial 70S ribosome, demonstrating that PKI has an affinity to the highly conserved tRNA binding sites on the ribosome (16).

The molecular mechanism of translation initiation by IGR IRESs is not fully understood. The current view is that upon formation of the 80S•IRES complex, the PKI is placed in the P site on the small subunit, in a manner mimicking the initiator methionyl-tRNA^{Met} and the AUG codon (6–8, 10, 17). In this mode, the IRES would position the ORF on the ribosome by presenting the initiating alanine codon in the A (aminoacyl) site.

Significance

Ribosomes decode genetic information encoded in mRNAs to synthesize cellular proteins. Initiation of translation is a key step, during which the ORF coding for a protein gets properly positioned on the ribosome with the AUG start codon and its cognate tRNA located in the ribosomal peptidyl site. Here, we report molecular structures of a eukaryotic ribosome complexed with viral mRNA, which uncover an unusual mechanism of initiation. The structures reveal that viral mRNAs carrying an intergenic RNA structure known as the internal ribosome entry site (IRES) initiate translation by binding a tRNA-mRNA–like element in the aminoacyl site of the ribosome. A structural mechanism of how viral mRNAs with intergenic IRESs hijack host ribosomes is proposed.

Author contributions: C.S.K., A.F.B., N.G., and A.A.K. designed research, performed research, analyzed data, and wrote the paper.

The authors declare no conflict of interest.

*This Direct Submission article had a prearranged editor.

Data deposition: Electron cryomicroscopy maps and structural models have been deposited in the EMDataBank (EMDB), www.emdatabank.org (EMDB ID codes EMD-5942 and EMD-5943), and the Protein Data Bank (PDB), www.pdb.org (PDB ID codes 3J6X and 3J6Y), respectively.

[1]C.S.K. and A.F.B. contributed equally to this work.

[2]To whom correspondence may be addressed. E-mail: andrei.korostelev@umassmed.edu or niko@grigorieff.org.

This article contains supporting information online at www.pnas.org/lookup/suppl/doi:10.1073/pnas.1406335111/-/DCSupplemental.

The structural studies of the mechanism, however, have been inconclusive. Previous electron cryomicroscopy (cryo-EM) reconstruction of the CrPV IRES bound to human ribosomal 40S subunit revealed the IRES density spanning from the A site to beyond the exit (E) site (18). The interpretation of the 40S•IRES map favored a model in which PKI interacts with the P-site region (18), although the 20-Å map lacked detailed features in this location. Cryo-EM studies of the 80S ribosome-bound CrPV IRES suggested that upon subunit joining and 80S•IRES complex formation, the IRES may rearrange relative to the 40S subunit (18), and/or reposition PKI in the vicinity of the A and P sites, yet potentially present the downstream alanine codon in the A site (19). The density for the PKI region in these 20-Å and 7.3-Å cryo-EM reconstructions was, however, significantly weaker than that for the rest of the CrPV IRES (18, 19), and it remained unclear how the IGR IRESs initiate translation by accurately positioning the ORF on the 80S ribosome. We report here ∼6-Å cryo-EM structures of the initiation 80S complex bound with an intergenic IRES, which provide structural insights into the mechanism of IGR IRES-driven initiation.

Results and Discussion

Structures of the TSV IRES Bound to the 80S Ribosome. To clarify the mechanism of translation initiation by IGR IRESs, we have determined cryo-EM structures of *Saccharomyces cerevisiae* 80S ribosome bound with the intergenic IRES RNA from Taura syndrome virus (TSV), whose structure has not been determined previously (Fig. 1 and Fig. S1). TSV is the etiological agent of Taura syndrome, which causes mortality in a number of shrimp species and has a significant negative impact on penaeid shrimp aquaculture worldwide (20). Whereas functionally similar, the *Aparavirus* family TSV IRES is structurally distinct from the better-characterized *Cripavirus* family CrPV and PSIV IRESs. Most notably, the PKI domain of the TSV IRES contains a hairpin-loop extension, stem loop III (SLIII) (Fig. 2 and Fig. S2), which is not present in CrPV and PSIV IRESs.

We have assembled the 80S•TSV IRES complex by incubating purified 40S and 60S subunits in the presence of the TSV IRES RNA (*Methods* and *SI Methods*). Upon classification of the cryo-EM data, two main conformations of the 80S•TSV IRES complex were identified (Fig. 1 and Fig. S1). Although the two complexes exhibit rotational states of the 40S subunit that differ by ∼3.5°, the conformations of the IRES RNA and its interactions with the ribosome in the two states are similar (Fig. 1 and Fig. S2). The 3-Å crystal structure of *S. cerevisiae* 80S ribosome (21) was used to model the molecular structure of the 80S•TSV IRES complex into our ∼6-Å cryo-EM maps (Fig. 1). Prominent density, which corresponds to the TSV IRES, spans the intersubunit space from the A site to beyond the E site (Figs. 1 and 3*A*). The cryo-EM maps allowed unambiguous fitting of the ribosome and TSV IRES domains, including PKI. The TSV IRES interacts with both subunits of the ribosome. The core of the double-nested pseudoknot domain of the IRES interacts with the ribosome in the vicinity of the P and E sites. SLIV and SLV of the double-nested pseudoknot domain are located outside of the E site, binding in the crevice between the head and platform of the 40S subunit (Fig. 3*A*). These interactions are similar to those made by the CrPV IRES (18, 19) and are described in *SI Text*.

PKI Occupies the Decoding Center on the Ribosome. The PKI domain forms a distinct structure, which is connected with the rest of the IRES via a "bridge" comprising PKII (Fig. 2). The codon-like CCU trinucleotide of the tRNA-mRNA–like PKI is placed more than 70 Å away from the tip of SLIV on the ribosome. Remarkably, whereas the double-nested pseudoknot domain contacts the ribosome primarily via ribosomal proteins, the PKI domain interacts predominantly with the ribosomal RNA (Fig. 2*C*). Upon formation of the 80S•IRES initiation complex, PKI was hypothesized to bind in the P site (2, 6–10, 17, 22–25) or between the A and P sites (19); however, previous structural studies have not reported the details of such occupancy due to low resolution or

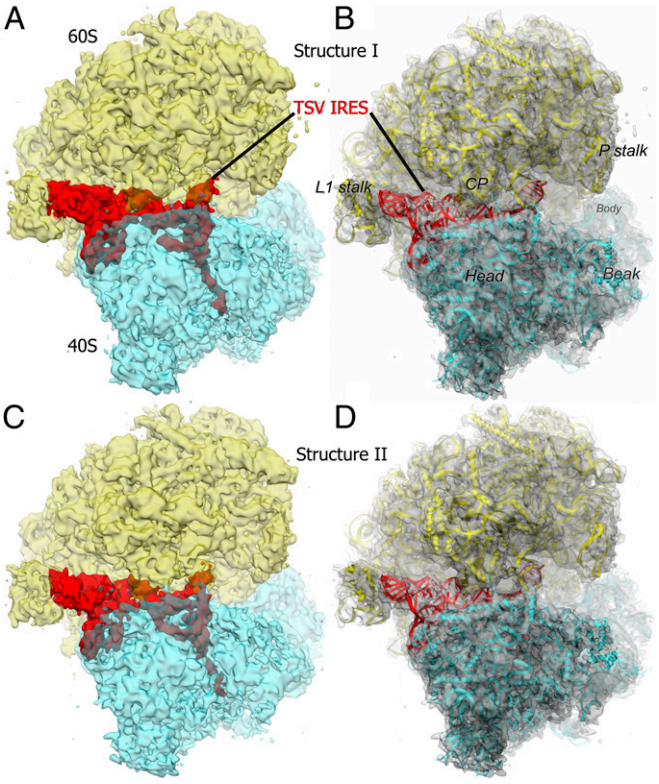

Fig. 1. Structures of the yeast 80S ribosome in complex with the TSV IRES RNA. (*A* and *C*) Cryo-EM maps of the 80S•TSV IRES complex (class I and class II) corresponding to structure I and structure II, respectively. The view is in the plane of the intersubunit interface, facing the head of the small subunit and the L1 stalk, central protuberance (CP), and P stalk of the large subunit. Density corresponding to the 60S ribosomal subunit is shown in yellow, that to the 40S subunit is shown in cyan, and that to IRES RNA is shown in red. (*B* and *D*) Ribbon representation of the 80S•TSV IRES structures I and II fitted into respective cryo-EM maps (transparent gray). The colors and views for the structural models in *B* and *D* are as in *A* and *C*.

weak map density in this region (18, 19). By contrast, the well-resolved density for PKI in our maps unambiguously reports that PKI is bound in the decoding center (A site) of the small subunit (Fig. 3). Here, the structure of the tRNA-mRNA–like portion of PKI closely resembles the A-site tRNA and mRNA in the crystal structures of tRNA-bound ribosome complexes (26–28). The direction of the helical axis of PKI, however, differs from that of the A-site tRNA by ∼10°. The shape of SLIII, which is coaxially stacked on PKI and extends toward the large ribosomal subunit, resembles that of the elbow of tRNA (Fig. 3*B*). Like the elbow of pre-translocation A-site tRNA (29), SLIII is positioned to interact with the A-site finger (ASF; nucleotides 1,008–1,043 of the 25S ribosomal RNA; Fig. 2). Due to a tilt in the helical axis of the PKI-SLIII helix, both the SLIII and ASF are shifted by ∼5 Å in comparison to the tRNA elbow and ASF of the 70S•tRNA complex or 80S•tRNA complex (Fig. S3*A*). During translocation of tRNA, the elbow of the A-tRNA must detour the ASF on its way toward the P site. It is likely that the contact between SLIII and ASF also contributes to the mechanism of translocation of the PKI-SLIII domain from the A site to the P site of the ribosome. In fact, deletion of SLIII of the TSV IRES did not significantly hamper the formation of the 40S•IRES and 80S•IRES complexes (13, 30), whereas the efficiency of in vitro translation was inhibited (30), consistent with the proposed role of SLIII in the initial positioning and/or translocation of the TSV IRES.

The conserved decoding center of the ribosome has been shown to undergo conformational changes during initiation, aminoacyl-tRNA accommodation, and termination of translation

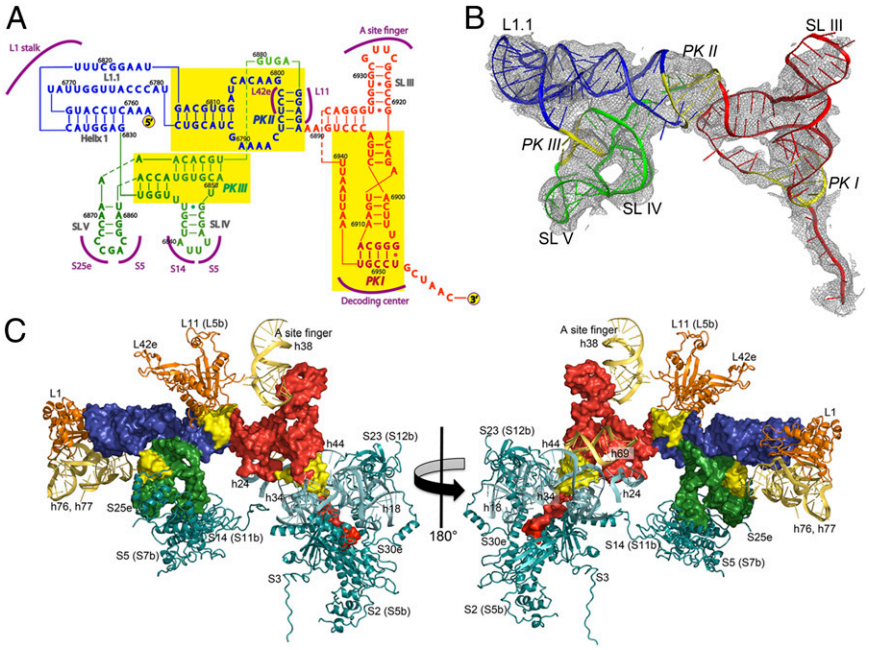

Fig. 2. Structural features of the TSV IRES RNA bound to the 80S ribosome. (*A*) Secondary structure of the TSV IRES RNA. The IRES is colored according to secondary structure features: Domains comprising PKI, PKII, and PKIII are shown in red, green, and blue, respectively. For the sake of clarity, all PKs are highlighted in yellow. The regions of the IRES that contact the ribosome are labeled in purple, with the text denoting the contact sites of the ribosome. (*B*) Ribbon representation of the TSV IRES RNA molecular structure fitted into the cryo-EM map (class I, gray mesh). Domains are colored as described in *A*, except that only the loop base-pairing part of each pseudoknot is in yellow. (*C*) Contacts of the TSV IRES RNA (surface-rendered and colored as in *B*) with the components of the ribosome (rendered as ribbons). Large-subunit ribosomal RNA and proteins are shown in yellow and orange, respectively; small-subunit ribosomal RNA and proteins are shown in cyan and teal, respectively. If bacterial homologs of ribosomal proteins exist and their names in the 80S and 70S ribosomes differ, bacterial protein names are followed by the letter "b" and specified in parentheses. Labels for eukaryote-specific proteins end with the letter "e."

(27, 31–33), all of which are essential for translation. The structural resemblance between PKI and the tRNA–mRNA interaction prompted us to investigate if the ribosomal decoding centers in the IRES- and tRNA-bound complexes are also similar. To this end, we compared our structures with the high-resolution crystal structure of the 70S ribosome bound with tRNA in the A site. In the tRNA-bound structure (27, 28), the universally conserved nucleotides A530, A1492, and A1493 of the small subunit and A1913 of helix 69 of the large subunit (*Escherichia coli* numbering) form specific interactions with the mRNA codon and tRNA anticodon stem loop (Fig. 3*D* and Fig. S4). These interactions were proposed to be critical for recognition of cognate tRNA by the ribosome (27). In our 80S•IRES structures, nucleotides G577, A1755, and A1756 (G530, A1492, and A1493 in *E. coli*) are also positioned to interact with the codon-anticodon–like helix of PKI (Fig. 3*E*). Specifically, A1755 and A1756 are retracted from their ground state (21) within helix 44 and contact the region comprising the first and second nucleotides of the mRNA-like CCU trinucleotide of PKI, which is placed in the A site (Fig. S4*D*). The tentative positions and conformations of the adenosines resemble those of bacterial A1492 and A1493, which form A-minor interactions with the first and second positions of the codon-anticodon helix in ribosome-tRNA crystal structures (28). In addition, A2256 (A1913 in *E. coli*) located at the tip of helix 69 of 25S rRNA contacts the anticodon-like part of PKI in a manner resembling that in tRNA-ribosome crystal structures (28, 29). In summary, the conformations of the decoding center in the 80S•TSV IRES complexes and during decoding of cognate tRNA by the ribosome closely resemble each other (Fig. 3 *D* and *E* and Fig. S4).

The initiating alanine codon GCU, which immediately follows PKI, is buried within the mRNA tunnel. The path of the downstream mRNA sequence is similar to that of canonical mRNA visualized in crystal structures of bacterial 70S ribosomes (21, 34). Specifically, the 3′ region of mRNA is placed in the mRNA entry tunnel between the head and body of the 40S subunit and interacts with ribosomal proteins S2 (S5 in bacteria), S3 (S3 in bacteria), and eukaryote-specific S30e on the solvent side of the 40S subunit (Fig. S5).

TSV IRES Stabilizes Two Partially Rotated Conformations of the Ribosome. The two conformations of the 80S•TSV IRES complex found by classification of our cryo-EM data (structures I and II; Fig. 1 and Fig. S1) differ by the relative positions of the ribosomal subunits, whereas the intrasubunit conformations are nearly identical. The global conformation of the small 40S subunit (relative positions of the head and the rest of the small subunit) is similar to that in the recently reported initiation 40S complex bound with initiation factor 1 (eIF1) and eIF1a [Protein Data Bank (PDB) ID code 4BPN], as discussed in *SI Text* (31). The transition between the 80S•TSV IRES ribosome conformations (from structure I to structure II) involves a concerted counterclockwise 3.5° rotation of the small subunit, IRES, and L1 stalk (Fig. 4) relative to the large subunit. The rotation takes place around intersubunit bridge B2c, formed in the vicinity of the A983:U1018 pair of the 18S rRNA, rpL43 and U2190 of 25S rRNA (21). This rotation results in an up to 5-Å displacement of the L1 stalk, whose interaction with L1.1 of the IRES remains preserved (Fig. 4, Fig. S6*A*, and *SI Text*). The concerted movement of the L1 stalk with the IRES implicates the involvement of this contact in IRES translocation, which echoes the role of the L1 stalk in the translocation of tRNA (35–37).

Ribosome dynamics play a crucial role in translation. Intersubunit rotation has been shown by structural, biochemical, and biophysical studies to be essential for concerted translocation of tRNA and mRNA in the course of elongation (38, 39). At least two globally dissimilar conformations of the ribosome have been identified by structural and FRET studies (40, 41). In the post-translocation state, in which peptidyl- and deacyl-tRNAs occupy the P and E sites, respectively, the ribosome adopts a "non-rotated" (classical) conformation. In the pretranslocation state, a 9–12° counterclockwise rotation of the small subunit was observed for bacterial (36, 42, 43) and eukaryotic (44) ribosomes. This conformation of the ribosome is referred to as "rotated." The peptidyl- and deacyl-tRNAs in the rotated pretranslocation ribosome are accommodated in the hybrid positions (45). Here, the anticodon stem loops are located in the A and P sites of the small subunit, whereas the acceptor arms on the large subunit are located in the P and E sites, respectively (41–43).

Because the IGR IRES mRNA has to undergo translocation to free its A site for alanyl-tRNA^{Ala}, we compared the conformational states of the IRES–ribosome complexes in our structures with the known pretranslocation (rotated) and posttranslocation-like (nonrotated) tRNA-bound rabbit ribosomes (44). As in bacterial ribosome complexes, the small subunit of the pretranslocation hybrid state mammalian ribosome is rotated counterclockwise by ~9° relative to that in the classical

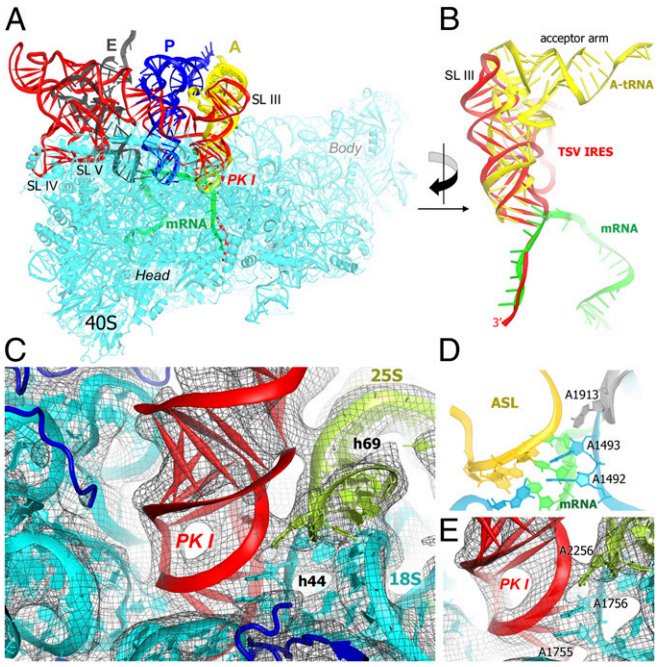

Fig. 3. Positioning of PKI in the decoding center of the ribosome is similar to that of the A-site tRNA and mRNA codon. (*A*) Comparison of the TSV IRES RNA (red) location on the 40S subunit (cyan) with tRNA positions in the A (yellow), P (blue), and E (gray) sites. Superposition was obtained by structural alignment of 16S ribosomal RNA from the crystal structure of a 70S•mRNA•tRNA complex containing three tRNAs (PDB ID code 3I8H) (29) with 18S ribosomal RNA of structure I (this work). (*B*) Comparison of PKI structure (red) with the mRNA (green) and tRNA (yellow) bound to the A site. (*C*) Structure of the decoding center of the 80S•TSV IRES complex fitted into the cryo-EM map (class I, gray mesh). PKI of the IRES RNA is shown in red, 18S rRNA is shown in cyan, 25S rRNA is shown in yellow-green, and ribosomal proteins are shown in blue. (*D*) Interactions of the anticodon stem loop of cognate tRNA (yellow) and mRNA (green) with the universally conserved elements of the decoding center in bacterial 70S ribosomes (29). The 16S rRNA is shown in cyan, and the 23S rRNA is shown in gray. (*E*) Interactions of PKI of the TSV IRES RNA with the decoding center of the 80S ribosome (this work), whose conformation resembles that of the tRNA-bound decoding center (*D*). Colors are as in *C*. A figure without mesh, showing the same view as in *E*, is presented in Fig. S4.

state ribosome (Fig. S6*B*). Comparison of the IRES-bound ribosome structures with the structures of rotated and nonrotated ribosomes reveals that the small subunit in both IRES-bound structures is in the intermediate state of rotation. Specifically, the small subunit is rotated counterclockwise by ~2° (structure I) and ~5° (structure II) relative to that in the classical state. Because the rotation of the small subunit in the IRES- and tRNA-bound complexes occurs along the same trajectory, the two rotational states of the 80S•IRES complex likely represent spontaneously sampled intermediates of the IRES translocation pathway.

Mechanistic Model for IGR IRES-Driven Initiation. Our structures lead us to propose a stepwise mechanism of translation initiation by Dicistroviridae IGR IRESs (Fig. 5). The uniform mechanism for *Cripavirus* and *Aparavirus* IRESs is strongly suggested by biochemical studies (5) and by the structural similarity revealed by this work for the CrPV and TSV IRESs. Here, the discussion of the initiation progression is supplemented by the results of published studies, which can now be explained in light of the proposed mechanism.

First, upon formation of the 40S•IRES complex, PKI of the IRES binds in the decoding center (Fig. 5*A*). Because no structural models are available for a 40S•IGR IRES complex, we have fitted the 40S subunit and the TSV IRES from our structures into the reported lower resolution cryo-EM density for the 40S•CrPV IRES complex (18) (Fig. S7). The fit demonstrates that the interaction of the IRES with the small subunit is similar to that in our 80S•IRES structures and confirms that PKI is occupying the A site in the 40S•IRES complex. Furthermore, the occupancy of the A site by PKI is supported by biochemical data as discussed in the next step.

Following the binding of the 60S subunit (Fig. 5*B*), additional contacts are formed between the IRES and the large subunit, including interactions with the L1 stalk in the E-site vicinity (Fig. S8) and protein L11 (homolog of bacterial L5) in the P site (Fig. 2*C*, Fig. S5, and *SI Text*). At this stage, PKI remains in the A site, consistent with numerous biochemical data, including those based on toe-printing. The toe-printing technique employs reverse transcription and reports the length of the primer-extension product resulting from blockage of reverse transcriptase by the ribosome. The method allows measurement of how many nucleotides separate an mRNA nucleotide of interest from the mRNA entrance point on the small subunit (46); thus, the position of the nucleotide of interest within the small subunit can be deduced from the results of toe-printing. Studies on CrPV, PSIV, and TSV IRESs have revealed that the location of the codon-like CCU trinucleotide of PKI on the small subunit is the same in the 40S•IRES and 80S•IRES complexes, demonstrating that PKI remains in the decoding center upon 80S•IRES complex formation (7, 10, 17). Furthermore, the distance from the first nucleotide of the codon-like trinucleotide of PKI (cytosine of the CCU in the TSV IRES, numbered +1) to the mRNA entrance is 12–13 nt, as the toe prints of +13 to +14 report (7, 10, 17). It is known from the studies on bacterial 70S•tRNA initiation complexes (46, 47), as well as on mammalian 80S ribosomes (48) bound with initiator methionyl-tRNA^{Met} and/or IRESs initiating with the canonical AUG codon, including the hepatitis C virus (49) and encephalomyocarditis virus (50) IRESs, that the toe prints of +16 to +17 correspond to the placement of the AUG codon in the P site. The toe prints of +13 to +14, observed for the PSIV, CrPV, and TSV IRESs on eukaryotic ribosomes (7, 10, 17), are therefore consistent with the placement of the CCU trinucleotide of PKI in the A site in both the 40S and 80S complexes. In this state, the alanine codon GCU is located in the mRNA tunnel, approaching the A site, as observed in our structures.

In the next step (Fig. 5*C*), the IRES has to be translocated by three nucleotides to bring the alanine codon into the A site and to vacate the A site for alanyl-tRNA^{Ala}. In agreement with this

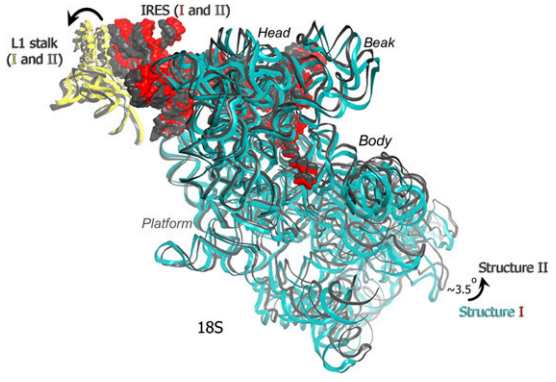

Fig. 4. Conformational differences between the two classes of the 80S•TSV IRES complex (structure I and structure II). Rotation of the small 40S subunit in structure II (gray) relative to that in structure I (teal) is coupled with rotation of the IRES (gray surface in structure II and red surface in structure I) and the L1 stalk of the large subunit (gray ribbon in structure II and yellow ribbon in structure I). The superposition was obtained by structural alignment of the 25S rRNA from the 80S•TSV IRES structure corresponding to structure I on that for structure II. The 40S subunit proteins are not shown for the sake of clarity.

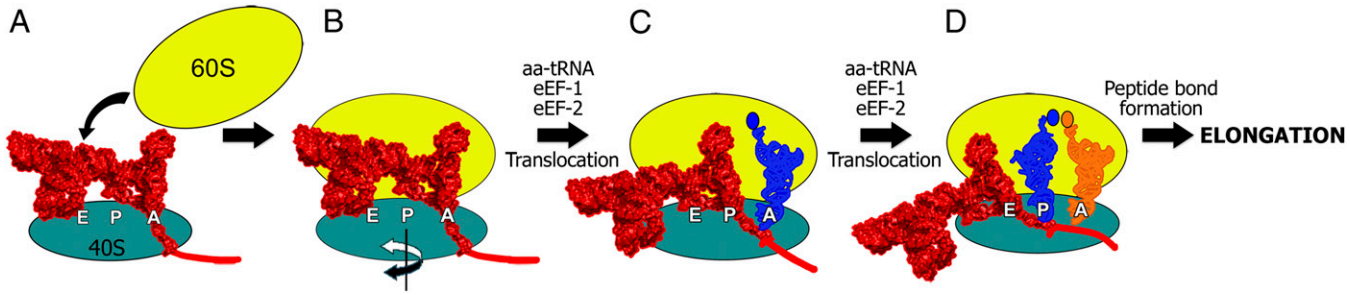

Fig. 5. Schematic of translation initiation by the IGR IRES RNA. (*A*) Formation of the 40S•IRES complex with PKI bound at the decoding center. (*B*) Subunit joining, resulting in the formation of 80S•IRES initiation complexes that sample distinct intersubunit conformations (this work). Spontaneous 40S subunit rotation, implicated in the downstream translocation event, is labeled with a double-headed arrow. (*C*) Translocation of the IRES RNA and accommodation of the first aminoacyl-tRNA (aa-tRNA) in the A site, catalyzed by eEF-1 and eEF-2. (*D*) Second translocation and accommodation of an aa-tRNA, resulting in an elongation-competent 80S complex. The 40S and 60S subunits are shown in teal and yellow, respectively; IRES RNA is shown in red; and tRNAs with their respective aminoacyl moieties (oval) are shown in blue and orange.

scheme, translocation of IGR IRESs by one codon was observed in toe-printing experiments, when alanyl-tRNA^{Ala} and eukaryotic elongation factor-1 (eEF-1) and eEF-2 were added to the 80S•IRES complex (17, 22, 30). In another set of experiments, the initiating alanine codon was mutated to a stop codon UAA to help identify the position of the codon by using eukaryotic release factor 1 (eRF1). When eRF1 was added together with the translocase eEF-2, translocation by one codon was observed (17). Because release factors bind to the ribosomal A site in response to a stop codon located in the decoding center (51, 52), these experiments demonstrate that PKI is originally positioned in the A site. Upon translocation, the following UAA codon is brought into the A site, allowing codon-specific binding of eRF1.

In the subsequent step of initiation by the IGR IRES (Fig. 5*D*), a second translocation event must take place to vacate the A site for the second tRNA. This positions the alanyl-tRNA^{Ala} in the P site and makes the ribosome complex functionally similar to the canonical initiation state complex, in which the initiator methionyl-tRNA^{Met} is bound in the P site. Consistent with this model, if the second codon of the ORF is replaced with the UAA stop codon in the experiments designed to involve eRF1 (17), two translocation events are required to bring this codon into the A site to allow eRF1 binding. In conclusion, in IGR IRES-driven initiation, binding of the second tRNA to the A site results in formation of the first peptide bond, thus commencing the elongation stage of translation (Fig. 5*D*).

The structures of the 80S•TSV IRES complexes show that in contrast to the mechanisms of canonical initiation or initiation driven by other groups of IRESs, IGR IRES-driven mRNAs must be translocated on the 80S ribosome two times to allow the first peptide bond to form. The molecular mechanism of the IGR IRES translocation is not known. Our observation of two rotational states of the IRES-bound 80S ribosome suggests that IGR IRES translocation employs spontaneous intersubunit rotation, mimicking, in part, the mechanism of tRNA and mRNA translocation (38, 41, 53). Specifically, eEF-2 likely rectifies the intersubunit rotation into translocation of PKI from the A site to the P site, conceptually resembling the mechanism of tRNA translocation by bacterial translocase elongation factor G (EF-G) (54). Intersubunit rotation in the IRES-bound initiation ribosome observed in our study (~3.5°) is, however, less pronounced than that in elongating tRNA-bound ribosomes (up to 12°), suggesting at least three scenarios for the mechanism of eEF-2–driven translocation of the IRES. First, additional conformational intermediates of the 80S•IRES complex may be spontaneously visited in solution, which sample a higher degree of intersubunit rotation and more closely resemble pretranslocation tRNA–ribosome complexes. Second, eEF2 may induce an additional rotation of the small subunit, as was recently observed for the bacterial pretranslocation EF-G–bound 70S•tRNA complex (54), and thus render the 80S•IRES•eEF2 pretranslocation complex conformationally and mechanistically closer to that in the tRNA translocation pathway. Third, it is possible that the global rearrangements of the ribosome resulting in the large 9–12° intersubunit rotation are not required in the course of initial IRES translocation. This is a plausible scenario because it is clear that the detailed structural mechanism of IRES movement within the ribosome must differ from that of tRNAs. During tRNA translocation, the acceptor arms of tRNA, which move sequentially from the A to P to E sites on the large subunit, play a crucial role (55) by enabling the formation of distinct tRNA intermediate states within the ribosome, such as classical and hybrid states (45). The distinct tRNA states depend on interactions of the acceptor arms with the conserved elements of the large subunit, including the peptidyl-transferase center, helix 68 located between the P and E sites (56), and helix 82 of the E site (28, 57). Because IGR IRESs do not bear acceptor-arm–like structures and do not interact with the acceptor-arm binding sites of the 60S subunit, it is not clear whether the translocating 80S•IRES complex samples conformations that are globally similar to those of tRNA-bound classical (0° rotation) and/or hybrid state (9–12° rotation) ribosomes. In summary, further experiments are required that address the conformational dynamics of the IGR IRES–ribosome complexes and tRNA (Fig. 5 *C* and *D*) and elongation factors to uncover the mechanism of IGR IRES translocation.

The P site is the bona fide binding site for the AUG start codon and initiator methionyl-tRNA^{Met} during canonical initiation. We have shown that the tRNA-mRNA–like PKI of the TSV IGR IRES is instead binding to the ribosomal decoding center, whereas the P site remains unoccupied. The structural analysis reveals that the position and interactions of PKI with the decoding center are similar to those of a cognate tRNA bound to the A site. Thus, our structures demonstrate a conceptually distinct mechanism for positioning the ORF on the ribosome, in which the decoding capacity of the ribosome is directly involved. This initiation mechanism may also be exploited by non-IGR IRES mRNAs. During canonical initiation, the P site is specific for initiator methionyl-tRNA^{Met} and efficiently discriminates against other tRNA species (58, 59). Cellular non–AUG-initiating mRNAs, such as those initiating with elongator tRNAs (60) or containing tRNA-like structural elements, may bypass the discriminatory P site by positioning the initiating codon-anticodon structure in the ribosomal decoding center.

Methods

A detailed description of the study methods can be found in *SI Methods*. The 80S ribosomes were prepared as described previously (21), from *S. cerevisiae* strain W303. The IRES–ribosome complex was assembled by incubating the IRES RNA with purified ribosomal subunits. Cryo-EM sample imaging and image processing were performed essentially as previously described (54). The TSV IRES RNA structural model was created using iterative prediction of secondary structure elements. Each 80S•TSV IRES structure was refined

against the corresponding map, using stereochemically restrained real-space refinement, essentially as described (54). Real-space R-factors are 0.195 and 0.197 for refined structures I and II, respectively, indicating good fits of the models to the maps.

ACKNOWLEDGMENTS. We thank A. Jacobson, R. Madireddy, and E. Mandon for providing reagents; A. Arif for initial work; Z. H. Yu and J. de la Cruz for help with collecting data; Y. X. Liao for help in picking particles; P. D. Zamore, R. Fukunaga, and E. Ricci for useful discussions; and D. N. Ermolenko, J. Kieft, and A. Korennykh for comments on the manuscript. The study was supported by grants from the Worcester Foundation for Biomedical Research, the University of Massachusetts Medical School Center for AIDS Research (to A.A.K.), and the Natural Sciences and Engineering Research Council (to A.F.B.) and by National Institutes of Health Grants R01 GM106105 (to A.A.K.) and P01 GM62580 (to N.G.).

1. Merrick WC (2004) Cap-dependent and cap-independent translation in eukaryotic systems. *Gene* 332:1–11.
2. Pestova TV, et al. (2001) Molecular mechanisms of translation initiation in eukaryotes. *Proc Natl Acad Sci USA* 98(13):7029–7036.
3. Balvay L, Soto Rifo R, Ricci EP, Decimo D, Ohlmann T (2009) Structural and functional diversity of viral IRESes. *Biochim Biophys Acta* 1789(9-10):542–557.
4. Hertz MI, Thompson SR (2011) Mechanism of translation initiation by Dicistroviridae IGR IRESs. *Virology* 411(2):355–361.
5. Hellen CU (2009) IRES-induced conformational changes in the ribosome and the mechanism of translation initiation by internal ribosomal entry. *Biochim Biophys Acta* 1789(9-10):558–570.
6. Jan E, et al. (2001) Initiator Met-tRNA-independent translation mediated by an internal ribosome entry site element in cricket paralysis virus-like insect viruses. *Cold Spring Harb Symp Quant Biol* 66:285–292.
7. Wilson JE, Pestova TV, Hellen CU, Sarnow P (2000) Initiation of protein synthesis from the A site of the ribosome. *Cell* 102(4):511–520.
8. Jan E, Sarnow P (2002) Factorless ribosome assembly on the internal ribosome entry site of cricket paralysis virus. *J Mol Biol* 324(5):889–902.
9. Nishiyama T, et al. (2003) Structural elements in the internal ribosome entry site of Plautia stali intestine virus responsible for binding with ribosomes. *Nucleic Acids Res* 31(9):2434–2442.
10. Cevallos RC, Sarnow P (2005) Factor-independent assembly of elongation-competent ribosomes by an internal ribosome entry site located in an RNA virus that infects penaeid shrimp. *J Virol* 79(2):677–683.
11. Hilbers CW, Michiels PJ, Heus HA (1998) New developments in structure determination of pseudoknots. *Biopolymers* 48(2-3):137–153.
12. Pfingsten JS, Costantino DA, Kieft JS (2006) Structural basis for ribosome recruitment and manipulation by a viral IRES RNA. *Science* 314(5804):1450–1454.
13. Pfingsten JS, Costantino DA, Kieft JS (2007) Conservation and diversity among the three-dimensional folds of the Dicistroviridae intergenic region IRESes. *J Mol Biol* 370(5):856–869.
14. Costantino DA, Pfingsten JS, Rambo RP, Kieft JS (2008) tRNA-mRNA mimicry drives translation initiation from a viral IRES. *Nat Struct Mol Biol* 15(1):57–64.
15. Kieft JS (2008) Viral IRES RNA structures and ribosome interactions. *Trends Biochem Sci* 33(6):274–283.
16. Zhu J, et al. (2011) Crystal structures of complexes containing domains from two viral internal ribosome entry site (IRES) RNAs bound to the 70S ribosome. *Proc Natl Acad Sci USA* 108(5):1839–1844.
17. Jan E, Kinzy TG, Sarnow P (2003) Divergent tRNA-like element supports initiation, elongation, and termination of protein biosynthesis. *Proc Natl Acad Sci USA* 100(26):15410–15415.
18. Spahn CM, et al. (2004) Cryo-EM visualization of a viral internal ribosome entry site bound to human ribosomes: The IRES functions as an RNA-based translation factor. *Cell* 118(4):465–475.
19. Schüler M, et al. (2006) Structure of the ribosome-bound cricket paralysis virus IRES RNA. *Nat Struct Mol Biol* 13(12):1092–1096.
20. Lightner DV, et al. (2012) Historic emergence, impact and current status of shrimp pathogens in the Americas. *J Invertebr Pathol* 110(2):174–183.
21. Ben-Shem A, et al. (2011) The structure of the eukaryotic ribosome at 3.0 Å resolution. *Science* 334(6062):1524–1529.
22. Yamamoto H, Nakashima N, Ikeda Y, Uchiumi T (2007) Binding mode of the first aminoacyl-tRNA in translation initiation mediated by Plautia stali intestine virus internal ribosome entry site. *J Biol Chem* 282(11):7770–7776.
23. Pestova TV, Hellen CU (2003) Translation elongation after assembly of ribosomes on the Cricket paralysis virus internal ribosomal entry site without initiation factors or initiator tRNA. *Genes Dev* 17(2):181–186.
24. Jackson RJ, Hellen CU, Pestova TV (2010) The mechanism of eukaryotic translation initiation and principles of its regulation. *Nat Rev Mol Cell Biol* 11(2):113–127.
25. Sarnow P, Cevallos RC, Jan E (2005) Takeover of host ribosomes by divergent IRES elements. *Biochem Soc Trans* 33(Pt 6):1479–1482.
26. Demeshkina N, Jenner L, Westhof E, Yusupov M, Yusupova G (2012) A new understanding of the decoding principle on the ribosome. *Nature* 484(7393):256–259.
27. Ogle JM, et al. (2001) Recognition of cognate transfer RNA by the 30S ribosomal subunit. *Science* 292(5518):897–902.
28. Selmer M, et al. (2006) Structure of the 70S ribosome complexed with mRNA and tRNA. *Science* 313(5795):1935–1942.
29. Jenner LB, Demeshkina N, Yusupova G, Yusupov M (2010) Structural aspects of messenger RNA reading frame maintenance by the ribosome. *Nat Struct Mol Biol* 17(5):555–560.
30. Jang CJ, Jan E (2010) Modular domains of the Dicistroviridae intergenic internal ribosome entry site. *RNA* 16(6):1182–1195.
31. Weisser M, Voigts-Hoffmann F, Rabl J, Leibundgut M, Ban N (2013) The crystal structure of the eukaryotic 40S ribosomal subunit in complex with eIF1 and eIF1A. *Nat Struct Mol Biol* 20(8):1015–1017.
32. Carter AP, et al. (2001) Crystal structure of an initiation factor bound to the 30S ribosomal subunit. *Science* 291(5503):498–501.
33. Korostelev AA (2011) Structural aspects of translation termination on the ribosome. *RNA* 17(8):1409–1421.
34. Yusupova G, Jenner L, Rees B, Moras D, Yusupov M (2006) Structural basis for messenger RNA movement on the ribosome. *Nature* 444(7117):391–394.
35. Cornish PV, et al. (2009) Following movement of the L1 stalk between three functional states in single ribosomes. *Proc Natl Acad Sci USA* 106(8):2571–2576.
36. Valle M, et al. (2003) Locking and unlocking of ribosomal motions. *Cell* 114(1):123–134.
37. Fei J, Kosuri P, MacDougall DD, Gonzalez RL, Jr. (2008) Coupling of ribosomal L1 stalk and tRNA dynamics during translation elongation. *Mol Cell* 30(3):348–359.
38. Horan LH, Noller HF (2007) Intersubunit movement is required for ribosomal translocation. *Proc Natl Acad Sci USA* 104(12):4881–4885.
39. Agirrezabala X, et al. (2012) Structural characterization of mRNA-tRNA translocation intermediates. *Proc Natl Acad Sci USA* 109(16):6094–6099.
40. Frank J, Agrawal RK (2000) A ratchet-like inter-subunit reorganization of the ribosome during translocation. *Nature* 406(6793):318–322.
41. Ermolenko DN, et al. (2007) Observation of intersubunit movement of the ribosome in solution using FRET. *J Mol Biol* 370(3):530–540.
42. Agirrezabala X, et al. (2008) Visualization of the hybrid state of tRNA binding promoted by spontaneous ratcheting of the ribosome. *Mol Cell* 32(2):190–197.
43. Julián P, et al. (2008) Structure of ratcheted ribosomes with tRNAs in hybrid states. *Proc Natl Acad Sci USA* 105(44):16924–16927.
44. Budkevich T, et al. (2011) Structure and dynamics of the mammalian ribosomal pretranslocation complex. *Mol Cell* 44(2):214–224.
45. Moazed D, Noller HF (1989) Intermediate states in the movement of transfer RNA in the ribosome. *Nature* 342(6246):142–148.
46. Hartz D, McPheeters DS, Gold L (1989) Selection of the initiator tRNA by Escherichia coli initiation factors. *Genes Dev* 3(12A):1899–1912.
47. Fredrick K, Noller HF (2002) Accurate translocation of mRNA by the ribosome requires a peptidyl group or its analog on the tRNA moving into the 30S P site. *Mol Cell* 9(5):1125–1131.
48. Schneider-Poetsch T, et al. (2010) Inhibition of eukaryotic translation elongation by cycloheximide and lactimidomycin. *Nat Chem Biol* 6(3):209–217.
49. Filbin ME, Vollmar BS, Shi D, Gonen T, Kieft JS (2013) HCV IRES manipulates the ribosome to promote the switch from translation initiation to elongation. *Nat Struct Mol Biol* 20(2):150–158.
50. Dmitriev SE, Pisarev AV, Rubtsova MP, Dunaevsky YE, Shatsky IN (2003) Conversion of 48S translation preinitiation complexes into 80S initiation complexes as revealed by toeprinting. *FEBS Lett* 533(1-3):99–104.
51. Chavatte L, Frolova L, Kisselev L, Favre A (2001) The polypeptide chain release factor eRF1 specifically contacts the s(4)UGA stop codon located in the A site of eukaryotic ribosomes. *Eur J Biochem* 268(10):2896–2904.
52. Taylor D, et al. (2012) Cryo-EM structure of the mammalian eukaryotic release factor eRF1-eRF3-associated termination complex. *Proc Natl Acad Sci USA* 109(45):18413–18418.
53. Ermolenko DN, Noller HF (2011) mRNA translocation occurs during the second step of ribosomal intersubunit rotation. *Nat Struct Mol Biol* 18(4):457–462.
54. Brilot AF, Korostelev AA, Ermolenko DN, Grigorieff N (2013) Structure of the ribosome with elongation factor G trapped in the pretranslocation state. *Proc Natl Acad Sci USA* 110(52):20994–20999.
55. Joseph S (2003) After the ribosome structure: How does translocation work? *RNA* 9(2):160–164.
56. Feinberg JS, Joseph S (2001) Identification of molecular interactions between P-site tRNA and the ribosome essential for translocation. *Proc Natl Acad Sci USA* 98(20):11120–11125.
57. Korostelev A, Trakhanov S, Laurberg M, Noller HF (2006) Crystal structure of a 70S ribosome-tRNA complex reveals functional interactions and rearrangements. *Cell* 126(6):1065–1077.
58. Lomakin IB, Shirokikh NE, Yusupov MM, Hellen CU, Pestova TV (2006) The fidelity of translation initiation: Reciprocal activities of eIF1, IF3 and YciH. *EMBO J* 25(1):196–210.
59. Kapp LD, Kolitz SE, Lorsch JR (2006) Yeast initiator tRNA identity elements cooperate to influence multiple steps of translation initiation. *RNA* 12(5):751–764.
60. Starck SR, et al. (2012) Leucine-tRNA initiates at CUG start codons for protein synthesis and presentation by MHC class I. *Science* 336(6089):1719–1723.

Supporting Information

Koh et al. 10.1073/pnas.1406335111

SI Text

Structural Interactions of the Taura Syndrome Virus Internal Ribosome Entry Site RNA with the Ribosome. At the 5′ region of intergenic region (IGR) internal ribosome entry sites (IRESs), pseudoknot III (PKIII) and PKII, which are critical for formation of the 40S•IRES and 80S•IRES complexes (1, 2), form a double-nested pseudoknot domain (3). The crystal structure of this region from the *Plautia stali* virus IGR IRES revealed that PKIII and PKII fold into a helical-stack core with two protruding stem loops, SLIV and SLV (4). The core is formed by two nearly parallel stacks of helices, which are connected through loop L1.1 (L1.1) (Fig. 2).

In our structures of the Taura syndrome virus (TSV) IRES bound to the 80S ribosome, the 5′-end of the IRES capped with helix 1 is located in the intersubunit space next to the L1 stalk of the 60S subunit. This location contrasts with that of canonical mRNA, whose single-stranded 5′ region occupies the mRNA exit tunnel of the small subunit (5, 6). The position of the IRES terminus more than 70 Å away from the narrow mRNA tunnel allows for the packing of the bulky structure of the 5′ end in the intersubunit space. Helix 1 is followed by L1.1, which interacts with the L1 stalk of the large ribosomal subunit (Figs. 1 and 4 and Figs. S6 and S8). This interaction is likely important at the stage of 60S subunit joining with the 40S•IRES complex. Indeed, mutations within the L1.1 region of the cricket paralysis virus (CrPV) and TSV IRESs do not interfere with formation of the 40S•IRES complex but disrupt 80S assembly and inhibit IRES-dependent translation (4, 7, 8). PKII, located downstream from L1.1, interacts with the C terminus of eukaryote-specific L42 and with rpL11 (Fig. 2). Notably, rpL11 and its bacterial counterpart L5 interact with the elbow of P-site tRNA in the tRNA-bound 80S and 70S ribosomes (9–11), respectively, underscoring the conserved roles of this protein–RNA contact in translation.

SLIV and SLV, whose loop sequences are conserved in the family of Dicistroviridae IRESs, are located outside of the E site on the periphery of the 40S subunit (Fig. S8). SLV is positioned farther from the E site and interacts with the head of the small subunit. The tip of SLV (nucleotides 6,859–6,871) is located in the crevice formed by ribosomal proteins rpS5 (rpS7 in *Escherichia coli*) and eukaryote-specific rpS25. This interaction is similar to that found by structural and cross-linking studies for CrPV IRES (12) and is critical for IGR IRES activity on yeast and mammalian ribosomes (13, 14). The second stem loop, SLIV, is joined with SLV via PKIII. The helical axes of these two stem loops are nearly perpendicular to each other, such that SLIV packs in the cleft between the head and platform of the small subunit (Fig. 4 and Figs. S6 and S8). Here, the tip of SLIV (nucleotides 6,836–6,847) interacts with rpS5 of the head region and rpS14 (rpS11 in *E. coli*) of the platform, likely contributing to stabilization of the conformation of the small ribosomal subunit as discussed below.

Conformation of the L1 Stalk in the 80S•IRES Complexes. The intersubunit rotation observed in our structures suggests a concerted change of the L1 stalk and IRES positions (Fig. 4 and Fig. S6). This motion implies a contact between the IRES and L1 stalk during IRES translocation, echoing the role of the L1 stalk in translocation of tRNA (15, 16). During tRNA translocation, the L1 stalk interacts with the elbow of tRNA and samples at least three conformations in the course of tRNA movement from the P site (17, 18). Specifically, studies on the 70S ribosome have shown that the L1 stalk rearranges from the fully closed state (contacting the hybrid state P/E tRNA) to the partially closed state (contacting E-site tRNA) and to the open state (coupled with tRNA exit from the ribosome). In the TSV IRES-bound complexes, the L1 stalk adopts a more open conformation than those in tRNA-bound or vacant ribosomes (Fig. S3 *B*–*E*). Here, the tip of the L1 stalk is more than 20 Å farther from the E site than in the ribosomes whose E site is occupied by tRNA (Fig. S3*E*).

Stabilization of the 40S Subunit Head Swivel by the TSV IRES. The conformations of the small subunit in the two 80S•TSV IRES complexes that we have visualized are nearly identical. Structural and biophysical studies of the bacterial ribosome demonstrated that the small ribosomal subunit undergoes intrasubunit rearrangements during translation, the most prominent of which involves movement of the head relative to the rest of the subunit (16). Head movement is implicated during at least three steps of translation: initiation, tRNA decoding, and translocation. Electron cryomicroscopy (Cryo-EM) studies (19) and recent crystal structures of the 40S subunit bound with eukaryotic initiation factor 1 (eIF1) and eIF1a (20) have revealed that binding of eIF1a next to the decoding center induces head rotation (swiveling). In the four crystal structures of the 40S•eIF1•eIF1a complex (20), there are four different states of head swivel. In comparison to the 40S•eIF1 complex (21), the head is swiveled by 4–12° toward the ribosomal E site when eIF1a is bound. This conformational change on the small subunit is hypothesized to contribute to the mechanism of subunit scanning along mRNA (19, 20, 22). Second, in addition to their role in initiation, intrasubunit rearrangements are implicated in tRNA decoding. In particular, binding of cognate tRNA to the decoding center of the bacterial ribosomes was shown to be coupled with "domain closure," whose mode is different from the head swivel (23, 24). Here, the beak of the small subunit moves toward the body by ∼4 Å as the small subunit forms contacts with the anticodon stem loop of tRNA (24). Third, structural studies of bacterial 70S ribosomes showed that head swivel plays a role in tRNA translocation through the ribosome (25–28). Head rotation likely contributes to translocation by widening the tRNA-mRNA channel on the small subunit between the P and E sites (28). As in bacterial 70S complexes, the head of the 40S subunit is modestly (by ∼2°) swiveled in the rotated rabbit 80S•tRNA ribosome with respect to its position in the nonrotated ribosome (11).

Because the 80S•IGR IRES complex represents an initiation state, a tRNA-bound state, and a pretranslocation state, we considered the possibility that binding of the IRES to the ribosome stabilizes a swiveled conformation and/or causes domain closure. The conformation of the small subunit closely resembles one of the four structures of the 40S•eIF1•eIF1a complexes [Protein Data Bank (PDB) ID code 4BPN] and is different from those in tRNA-bound complexes (11). In particular, the head is rotated by ∼8° toward the E site in comparison to its position in the tRNA-bound nonrotated ribosome. As such, the head "slides" in the vicinity of the aminoacyl (A) site by up to 6 Å, in the direction perpendicular to that of domain closure. This conformation of the head is stabilized by interactions of SLIV with the cleft between the head and the platform (described above), and is permissive for accommodation of PKI in the A site. Indeed, structure superpositions show that conformations of the 40S subunit in the free state (21) or tRNA-bound state (22) are not compatible with IRES binding because the PKI would sterically clash with the head in several positions.

SI Methods

Preparation of the 80S•TSV IRES Complex. The 80S ribosomes used in this study were prepared as described previously (5), from *Saccharomyces cerevisiae* strain W303. To obtain ribosomal subunits, purified 80S was incubated in dissociation buffer containing 20 mM Hepes K (pH 7.5; OmniPur), 0.5 M KCl (Fisher Scientific), 1 mM $Mg(OAc)_2$ (J. T. Baker), 2 mM DTT (Enzo Life Science), and 0.5 U/μL RNasin (Promega) for 1 h at 4 °C. The dissociated subunits were then layered on sucrose gradients (10–30% sucrose; Mallinckrodt Chemicals) in the dissociation buffer and centrifuged for 15 h at 22,000 rpm in an SW32 Ti Beckman Coulter rotor [corresponding to the relative centrifugal forces of 82667 (RCF maximum) and 59439 (RCF average)]. Fractions corresponding to 40S and 60S subunits were pooled and buffer-exchanged to subunit storage buffer containing 50 mM Tris (pH 7.5; Fischer Scientific), 20 mM $MgCl_2$ (OmniPur), 100 mM KCl, and 2 mM DTT. Purified subunits were stored in small portions at −80 °C.

Synthetic DNA encoding for nucleotides 6,741–6,990 of the TSV mRNA sequence inserted into pUC57 (Genscript) was used to amplify the 250-nt fragment by PCR. This DNA fragment encodes for the TSV IRES RNA and served as a template for the in vitro transcription reaction. The TSV IRES RNA in vitro transcript was synthesized by recombinant T7 RNA polymerase, using the DNA template resulting from the PCR. A transcription reaction was incubated for 5 h at 37 °C before the resulting transcription product was treated with DNase I (New England Biolabs) for 30 min at 37 °C. The RNA was then extracted using acidic phenol/chloroform (Ambion). The RNA was further gel-purified and ethanol-precipitated with 100% ethanol (Decon Laboratories), followed by an 80% ethanol wash. The resulting RNA pellet was air-dried at room temperature and suspended in RNase-free water.

The TSV IRES RNA (4.8 μM final concentration) was refolded in the final 80S•TSV IRES storage buffer containing 45 mM Hepes·KOH (pH 7.5), 10 mM $MgCl_2$, 100 mM KCl, 2.5 mM spermine (Alfa Aesar), 2 mM β-mercaptoethanol (Alfa Aesar), and 0.5 U/μL RNasin for 5 min at 65 °C and cooled for 30 min at room temperature before ribosome complex formation. The IRES–ribosome complex was assembled in two steps. First, the TSV IRES RNA was incubated with the 40S small subunit (0.6 μM) for 15 min at 30 °C. Subsequently, the yeast 60S large subunit (0.3 μM) was added and incubated for an additional 15 min at 30 °C. Complexes were transferred to ice for 5 min and then flash-frozen in liquid nitrogen.

Grids for cryo-EM were prepared essentially as described (29), with minor modifications. Ribosomal complexes were thawed on ice immediately before plunging. Approximately 2 μL of undiluted sample was applied to freshly glow-discharged, 400-mesh, C-flat 1.2–1.3 grids using an FEI Mark II Vitrobot.

EM. Sample imaging was performed essentially as previously described (29). The nominal defocus was varied from 2.0 to 3.5 μm of underfocus. Images were collected on a Falcon I direct electron detector (FEI), with a total dose of 30 electrons per square angstrom and a calibrated pixel size on the specimen of 1.0595 Å.

Image Processing. Image processing was performed essentially as described (29, 30). Particles were semiautomatically selected using e2boxer's swarm tool (31), followed by manual curation of the dataset. This semiautomatic particle picking excluded the majority of 40S particles that could be seen in micrographs. Defocus parameters were determined using CTFFIND3 (32). Boxing was performed using batchboxer (33), with unbinned images having a box size of 420 pixels.

Initial alignment parameters were assigned using IMAGIC (34), essentially as described (29). Boxed particles were normalized to have a constant variance and zero average, fivefold-binned and phase-flipped to account for the contrast transfer function, band pass-filtered with cutoffs of 0.02 and 0.2, and masked with a soft circular mask with a radius of 0.62 (fraction of one-half of the image size) and a fall-off of 0.08.

Particle images were aligned against a published 80S ribosome structure (12) (EMDataBank (EMDB) ID code EMD-1285).

Further processing with FREALIGN (30) was carried out as described (29) using unfiltered images. The data were refined against a single reference until no further improvement was seen in resolution, as indicated by the calculated Fourier shell correlation (FSC) between rounds. Refinement included data up to 35 Å initially and data at higher resolution as refinement progressed, up to a resolution 7.7 Å in the final round of refinement. Threefold binned data were then divided into eight classes using RSAMPLE (part of the FREALIGN software package, http://grigoriefflab.janelia.org/frealign) (35), and classified without refining the alignment parameters, while including data between 150 and 12 Å. This yielded six classes with recognizable features at high resolution (36) (better than 12 Å, FSC = 0.143). Two of these classes showed continuous density corresponding to the TSV IRES (Fig. 1 and Fig. S1).

Particles belonging to these two classes were then extracted from the dataset and further refined against a single reference using FREALIGN and optimal filtering (37). The refinement included data from 150 to 14 Å initially, and up to a resolution of 10 Å in the final rounds of refinement.

The resolution of the classes shown in Fig. S1 was assessed using masked semi-independent half-volumes generated by FREALIGN, yielding a resolution of about 6 Å for both maps (FSC = 0.143 criterion). Briefly, a generous mask with a seven-pixel fall-off was generated from the final volumes using the automask3d processor in EMAN2 (31) and applied to both half-volumes before determination of the FSC. Additionally, an FSC measurement was generated using the optimal filtering procedure in FREALIGN (37) for classes I and II. As was observed in previous cryo-EM studies (38), the core of the ribosome is resolved somewhat better than the peripheral parts. We used the program ResMap (version 1.1.4) (39) to estimate local resolution using split volumes as an input. We subsequently found that the core regions of the ribosomal subunits are resolved at somewhat better resolution than 6 Å, as is evident from the well-defined secondary structure features. The region around domain 3 of the IRES is resolved at about 6.5 Å, and the resolution of other parts of the IRES is estimated to be somewhat lower than this, likely reflecting the conformational flexibility of IRES domains.

Fitting of the 80S•TSV IRES Structural Models into Cryo-EM Maps. The TSV IRES RNA structure was created using iterative prediction of secondary structure elements by RNAifold (40) and ModeRNA (41), followed by modeling of these elements into the cryo-EM maps. The structure prediction and modeling were aided by the published crystal structures of IGR IRES domains (4, 42) and the cryo-EM structure of the CrPV IRES bound to the 80S ribosome (12). The 3.0-Å crystal structure of the 80S ribosome (5) was fitted into the cryo-EM maps using Chimera, and each 80S•TSV IRES structure was then independently refined against the maps using the stereochemically restrained, rigid body, real-space refinement package RSRef (43–45) implemented as a module of CNS (Crystallography and NMR System) (46), essentially as described (29). The structure of rpL1 was obtained by homology modeling from PDB ID code 3J3B (38), using the SWISS-MODEL server (47). During rigid body refinement, the IRES RNA structure was split into rigid body domains comprising secondary structure elements. To fit the decoding center structure accurately into the cryo-EM maps, whose resolution is not sufficient to resolve A1755 and A1756 individually, the universally conserved nucleotides from the crystal structure of the bacterial 70S•tRNA complex (23) were placed in the 80S•IRES starting models. At the final stage of structure optimization, both

80S•IRES structures were subjected to stereochemically restrained real-space refinement, facilitated by base-pairing and base-stacking restraints, as described (48). Relative weights for stereochemical restraints and the experimental term (agreement with cryo-EM density) were optimized at each step of refinement to yield proper structural models. In the refined structures, small deviations from ideal stereochemical parameters [rmsd (covalent bond lengths) of ~0.01 Å and rmsd (covalent bond angles) of ~1.2°] indicate good stereochemical geometry of structural models and the suitability of models for structural interpretations. All-atom rms differences between 25S rRNA of the refined structures and the starting 3-Å crystal structure (excluding the mobile L1 stalk, P stalk, and A-site finger) are 1.1 Å (for structure I) and 1.2 Å (for structure II), consistent with the average coordinate error of ~1 Å for the cryo-EM structural models, similar to the expected coordinate error of cryo-EM structures at a resolution of ~6 Å (49). Real-space R-factors, calculated in RSRef and reporting on disagreement between the structural model and experimental maps, are 0.195 and 0.197 for refined structures I and II, respectively, indicating a good fit of the models to the map. Structural alignments were performed in PyMOL (50). The axis of rotation of the small subunit between structures I and II was calculated using Chimera (51). Figures were rendered in PyMOL and Chimera (51).

1. Jan E, Sarnow P (2002) Factorless ribosome assembly on the internal ribosome entry site of cricket paralysis virus. *J Mol Biol* 324(5):889–902.
2. Nishiyama T, et al. (2003) Structural elements in the internal ribosome entry site of Plautia stali intestine virus responsible for binding with ribosomes. *Nucleic Acids Res* 31(9):2434–2442.
3. Hilbers CW, Michiels PJ, Heus HA (1998) New developments in structure determination of pseudoknots. *Biopolymers* 48(2-3):137–153.
4. Pfingsten JS, Costantino DA, Kieft JS (2006) Structural basis for ribosome recruitment and manipulation by a viral IRES RNA. *Science* 314(5804):1450–1454.
5. Ben-Shem A, et al. (2011) The structure of the eukaryotic ribosome at 3.0 Å resolution. *Science* 334(6062):1524–1529.
6. Yusupova G, Jenner L, Rees B, Moras D, Yusupov M (2006) Structural basis for messenger RNA movement on the ribosome. *Nature* 444(7117):391–394.
7. Pfingsten JS, Castile AE, Kieft JS (2010) Mechanistic role of structurally dynamic regions in Dicistroviridae IGR IRESs. *J Mol Biol* 395(1):205–217.
8. Jang CJ, Jan E (2010) Modular domains of the Dicistroviridae intergenic internal ribosome entry site. *RNA* 16(6):1182–1195.
9. Korostelev A, Trakhanov S, Laurberg M, Noller HF (2006) Crystal structure of a 70S ribosome-tRNA complex reveals functional interactions and rearrangements. *Cell* 126(6):1065–1077.
10. Selmer M, et al. (2006) Structure of the 70S ribosome complexed with mRNA and tRNA. *Science* 313(5795):1935–1942.
11. Budkevich T, et al. (2011) Structure and dynamics of the mammalian ribosomal pretranslocation complex. *Mol Cell* 44(2):214–224.
12. Schüler M, et al. (2006) Structure of the ribosome-bound cricket paralysis virus IRES RNA. *Nat Struct Mol Biol* 13(12):1092–1096.
13. Hertz MI, Landry DM, Willis AE, Luo G, Thompson SR (2013) Ribosomal protein S25 dependency reveals a common mechanism for diverse internal ribosome entry sites and ribosome shunting. *Mol Cell Biol* 33(5):1016–1026.
14. Landry DM, Hertz MI, Thompson SR (2009) RPS25 is essential for translation initiation by the Dicistroviridae and hepatitis C viral IRESs. *Genes Dev* 23(23):2753–2764.
15. Korostelev A, Ermolenko DN, Noller HF (2008) Structural dynamics of the ribosome. *Curr Opin Chem Biol* 12(6):674–683.
16. Frank J, Gonzalez RL, Jr. (2010) Structure and dynamics of a processive Brownian motor: The translating ribosome. *Annu Rev Biochem* 79:381–412.
17. Cornish PV, et al. (2009) Following movement of the L1 stalk between three functional states in single ribosomes. *Proc Natl Acad Sci USA* 106(8):2571–2576.
18. Fei J, Kosuri P, MacDougall DD, Gonzalez RL, Jr. (2008) Coupling of ribosomal L1 stalk and tRNA dynamics during translation elongation. *Mol Cell* 30(3):348–359.
19. Passmore LA, et al. (2007) The eukaryotic translation initiation factors eIF1 and eIF1A induce an open conformation of the 40S ribosome. *Mol Cell* 26(1):41–50.
20. Weisser M, Voigts-Hoffmann F, Rabl J, Leibundgut M, Ban N (2013) The crystal structure of the eukaryotic 40S ribosomal subunit in complex with eIF1 and eIF1A. *Nat Struct Mol Biol* 20(8):1015–1017.
21. Rabl J, Leibundgut M, Ataide SF, Haag A, Ban N (2011) Crystal structure of the eukaryotic 40S ribosomal subunit in complex with initiation factor 1. *Science* 331(6018):730–736.
22. Lomakin IB, Steitz TA (2013) The initiation of mammalian protein synthesis and mRNA scanning mechanism. *Nature* 500(7462):307–311.
23. Demeshkina N, Jenner L, Westhof E, Yusupov M, Yusupova G (2012) A new understanding of the decoding principle on the ribosome. *Nature* 484(7393):256–259.
24. Ogle JM, et al. (2001) Recognition of cognate transfer RNA by the 30S ribosomal subunit. *Science* 292(5518):897–902.
25. Pulk A, Cate JH (2013) Control of ribosomal subunit rotation by elongation factor G. *Science* 340(6140):1235970.
26. Ratje AH, et al. (2010) Head swivel on the ribosome facilitates translocation by means of intra-subunit tRNA hybrid sites. *Nature* 468(7324):713–716.
27. Zhou J, Lancaster L, Donohue JP, Noller HF (2013) Crystal structures of EF-G-ribosome complexes trapped in intermediate states of translocation. *Science* 340(6140):1236086.
28. Schuwirth BS, et al. (2005) Structures of the bacterial ribosome at 3.5 A resolution. *Science* 310(5749):827–834.
29. Brilot AF, Korostelev AA, Ermolenko DN, Grigorieff N (2013) Structure of the ribosome with elongation factor G trapped in the pretranslocation state. *Proc Natl Acad Sci USA* 110(52):20994–20999.
30. Grigorieff N (2007) FREALIGN: High-resolution refinement of single particle structures. *J Struct Biol* 157(1):117–125.
31. Tang G, et al. (2007) EMAN2: An extensible image processing suite for electron microscopy. *J Struct Biol* 157(1):38–46.
32. Mindell JA, Grigorieff N (2003) Accurate determination of local defocus and specimen tilt in electron microscopy. *J Struct Biol* 142(3):334–347.
33. Ludtke SJ, Baldwin PR, Chiu W (1999) EMAN: Semiautomated software for high-resolution single-particle reconstructions. *J Struct Biol* 128(1):82–97.
34. Van Heel M, et al. (2011) Four-dimensional cryo electron microscopy at quasi atomic resolution: 'IMAGIC 4D'. *International Tables for Crystallography*, eds Arnold E, Himmel DM, Rossmann MG (John Wiley and Sons, New York), Vol F: Crystallography of Biological Macromolecules, pp 624–628.
35. Lyumkis D, Brilot AF, Theobald DL, Grigorieff N (2013) Likelihood-based classification of cryo-EM images using FREALIGN. *J Struct Biol* 183(3):377–388.
36. Rosenthal PB, Henderson R (2003) Optimal determination of particle orientation, absolute hand, and contrast loss in single-particle electron cryomicroscopy. *J Mol Biol* 333(4):721–745.
37. Sindelar CV, Grigorieff N (2011) An adaptation of the Wiener filter suitable for analyzing images of isolated single particles. *J Struct Biol* 176(1):60–74.
38. Anger AM, et al. (2013) Structures of the human and Drosophila 80S ribosome. *Nature* 497(7447):80–85.
39. Kucukelbir A, Sigworth FJ, Tagare HD (2014) Quantifying the local resolution of cryo-EM density maps. *Nat Methods* 11(1):63–65.
40. Garcia-Martin JA, Clote P, Dotu I (2013) RNAiFold: A web server for RNA inverse folding and molecular design. *Nucleic Acids Res* 41(Web Server issue): W465–W470.
41. Rother M, et al. (2011) ModeRNA server: An online tool for modeling RNA 3D structures. *Bioinformatics* 27(17):2441–2442.
42. Costantino DA, Pfingsten JS, Rambo RP, Kieft JS (2008) tRNA-mRNA mimicry drives translation initiation from a viral IRES. *Nat Struct Mol Biol* 15(1):57–64.
43. Korostelev A, Bertram R, Chapman MS (2002) Simulated-annealing real-space refinement as a tool in model building. *Acta Crystallogr D Biol Crystallogr* 58(Pt 5): 761–767.
44. Fabiola F, Chapman MS (2005) Fitting of high-resolution structures into electron microscopy reconstruction images. *Structure* 13(3):389–400.
45. Chen JZ, Fürst J, Chapman MS, Grigorieff N (2003) Low-resolution structure refinement in electron microscopy. *J Struct Biol* 144(1-2):144–151.
46. Brünger AT, et al. (1998) Crystallography & NMR system: A new software suite for macromolecular structure determination. *Acta Crystallogr D Biol Crystallogr* 54(Pt 5): 905–921.
47. Arnold K, Bordoli L, Kopp J, Schwede T (2006) The SWISS-MODEL workspace: A web-based environment for protein structure homology modelling. *Bioinformatics* 22(2): 195–201.
48. Laurberg M, et al. (2008) Structural basis for translation termination on the 70S ribosome. *Nature* 454(7206):852–857.
49. Rossmann MG (2000) Fitting atomic models into electron-microscopy maps. *Acta Crystallogr D Biol Crystallogr* 56(Pt 10):1341–1349.
50. DeLano WL (2002) *The PyMOL Molecular Graphics System* (DeLano Scientific, Palo Alto, CA).
51. Pettersen EF, et al. (2004) UCSF Chimera—A visualization system for exploratory research and analysis. *J Comput Chem* 25(13):1605–1612.
52. Spahn CM, et al. (2004) Cryo-EM visualization of a viral internal ribosome entry site bound to human ribosomes: The IRES functions as an RNA-based translation factor. *Cell* 118(4):465–475.

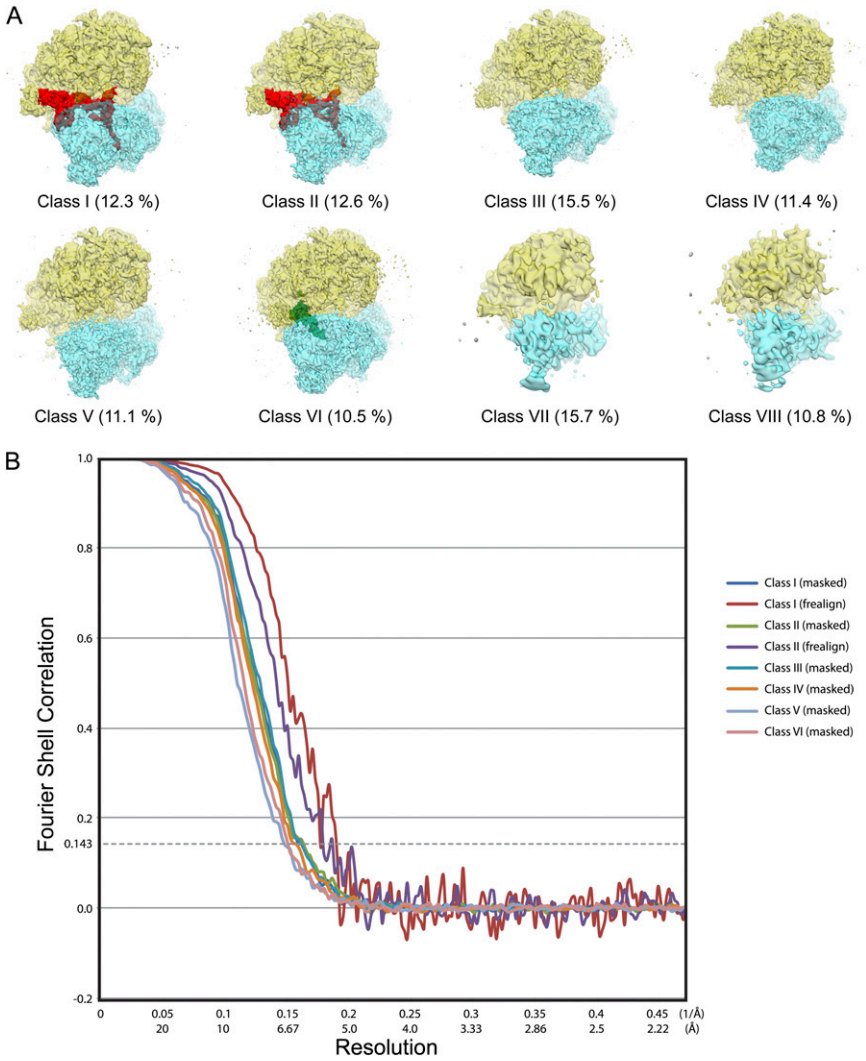

Fig. S1. Single-particle classification of cryo-EM data. (*A*) Sorting of 416,312 particle images resulted in eight classes, of which six showed high-resolution features consistent with an 80S ribosome structure: classes I and II, 80S ribosome with a bound TSV IRES; classes III, IV, and V, empty 80S ribosome; class VI, 80S ribosome with tRNA-like density in the P/E site; and classes VII and VIII, low-quality classes. (*B*) Fourier shell correlation curves for classes I–VI. For convenience, the *x* axis is labeled with both spatial frequency (0 to 0.45 $Å^{-1}$) and in angstroms (0 to 2.22 Å).

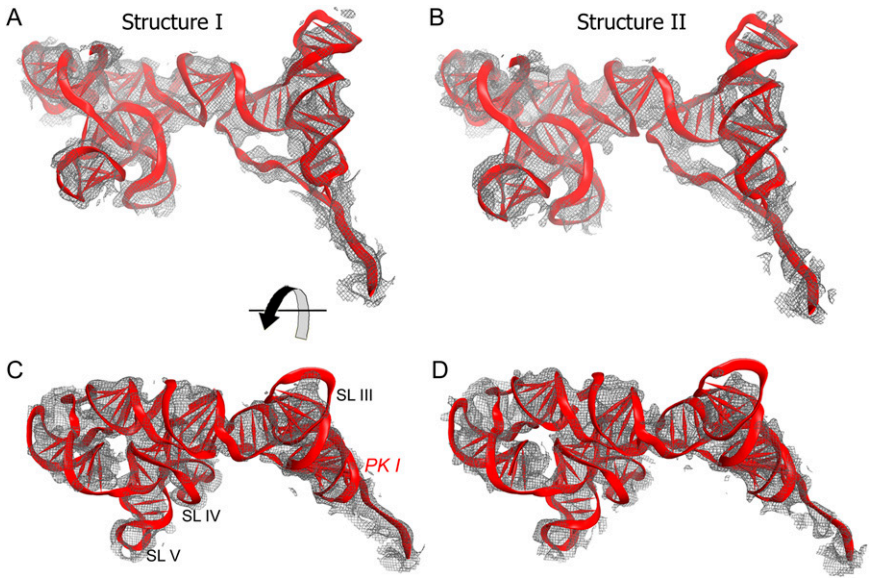

Fig. S2. Fit of the refined TSV IRES structure (red) to the cryo-EM maps (gray) for the ribosome-bound IRES complexes in structure I (*A* and *C*) and structure II (*B* and *D*). Secondary structure elements comprising PKI and SLIII, SLIV, and SLV are labeled for reference.

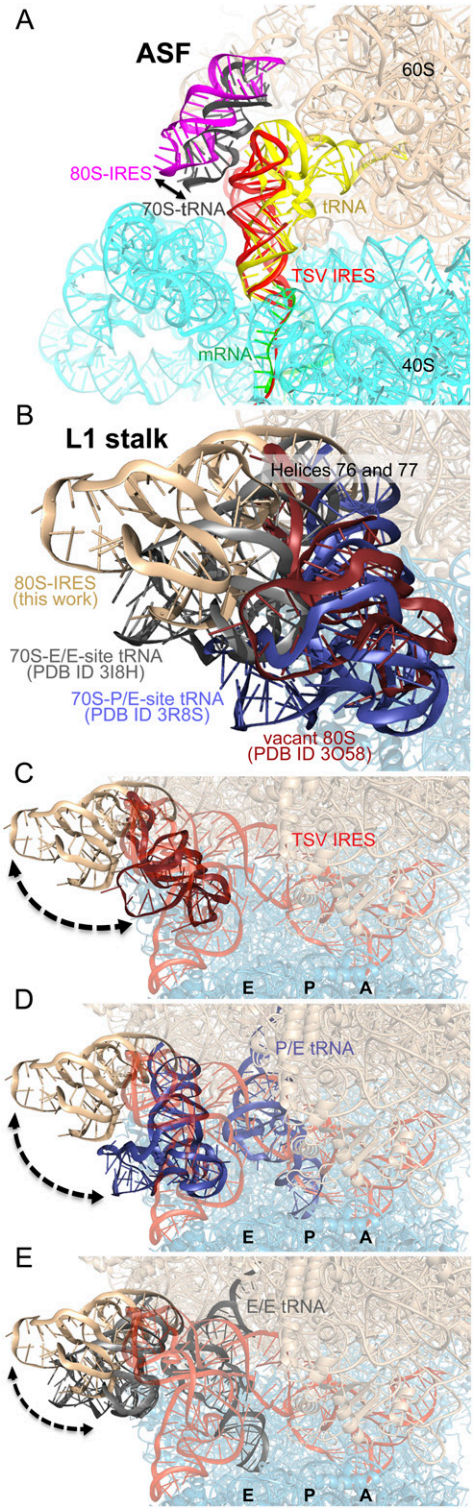

Fig. S3. Rearrangements of helix 38 [A-site finger (ASF)] and the L1 stalk in the IRES-bound ribosomes relative to those in tRNA-bound ribosome complexes. (*A*) TSV IRES RNA induces a shift of the ASF (magenta) in the 80S ribosome (this work; PDB ID code 3J6Y) relative to its position (gray) in the 70S ribosome (PDB ID codes 3I8H and 3I8I) bound with mRNA (green) and tRNA (yellow). For reference, ribosomal RNA of the large 60S subunit is shown in a wheat color and that of the small 40S subunit is shown in cyan. (*B*) Comparison of positions of the L1 stalk in the IRES-bound ribosome (wheat; this work), crystal structure of vacant 80S ribosome (ruby; PDB ID code 3O58), crystal structures of the 70S ribosome bound with hybrid state P/E tRNA (blue; PDB ID code 3R8S), and classical state E-tRNA (gray; PDB ID code 3I8H). L1 protein is omitted from the figures for the sake of clarity. (*C*) Comparison of positions of the L1 stalk in the IRES-bound ribosome (wheat; this work) and crystal structure of the 80S ribosome, whose E site is not occupied (ruby; PDB ID code 3O58). (*D*) Comparison of positions of the L1 stalk, IRES, and tRNA in the IRES-bound ribosome (wheat; this work) and crystal structure of the 70S ribosome bound with hybrid state P/E tRNA (blue; PDB ID code 3R8S). (*E*) Comparison of positions of the L1 stalk, IRES, and tRNA in the IRES-bound ribosome (wheat; this work) and crystal structure of the 70S ribosome bound with the E-tRNA (gray; PDB ID code 3I8H). For the sake of clarity, classical P/P tRNA is not shown in this panel. Superpositions were obtained by structural alignments of small-subunit ribosomal RNA from respective ribosome complexes. Ribosomal subunits in *C*, *D*, and *E* are colored as in *B*.

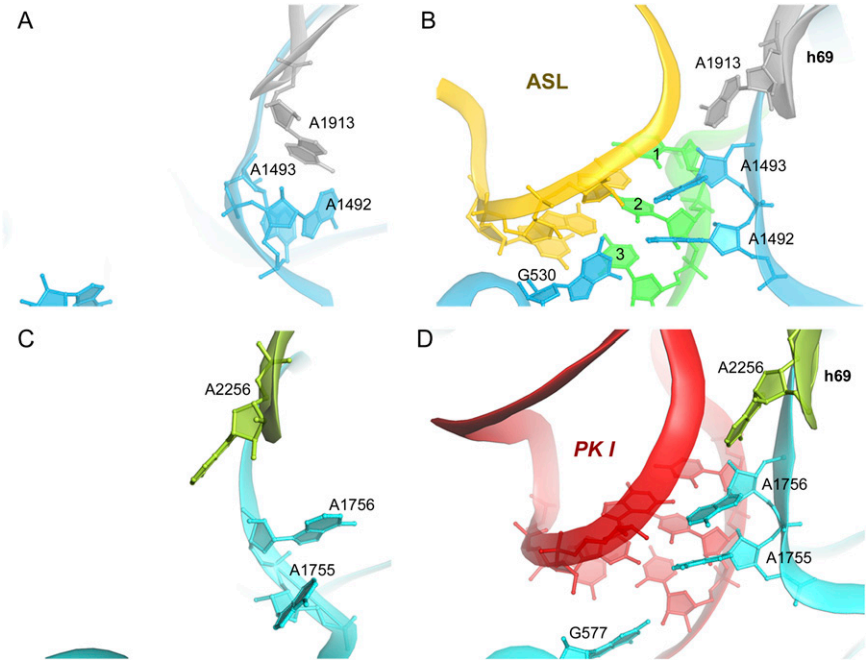

Fig. S4. Conformational rearrangements of universally conserved elements of the decoding center upon binding of tRNA or TSV IRES RNA. (*A*) Conformation of the 70S ribosomal decoding center in the absence of tRNA (PDB ID codes 3R8S and 4GD1). The 16S ribosomal RNA is shown in dark cyan, and helix 69 of 23S rRNA is shown in gray. (*B*) Interactions of the anticodon stem loop of cognate tRNA (yellow) and mRNA (green) with the universally conserved elements of the decoding center in bacterial 70S ribosomes (PDB ID codes 3I8H and 3I8I). Nucleotides of the A-site mRNA codon are labeled with numbers. (*C*) Conformation of the 80S ribosomal decoding center in the absence of tRNA or IRES (PDB ID codes 3U5B and 3U5D). The 25S ribosomal RNA is shown in yellow-green, and the 18S ribosomal RNA is shown in cyan. (*D*) Position and interactions of PKI of the TSV IRES (red) in the 80S decoding center (this work). Nucleotides A1755 and A1756 change positions relative to those in the vacant ribosome (*C*) upon binding of the IRES to the ribosome, thus resembling the behavior of their analogs A1492 and A1493 in the bacterial ribosome upon binding of cognate tRNA (*A* and *B*).

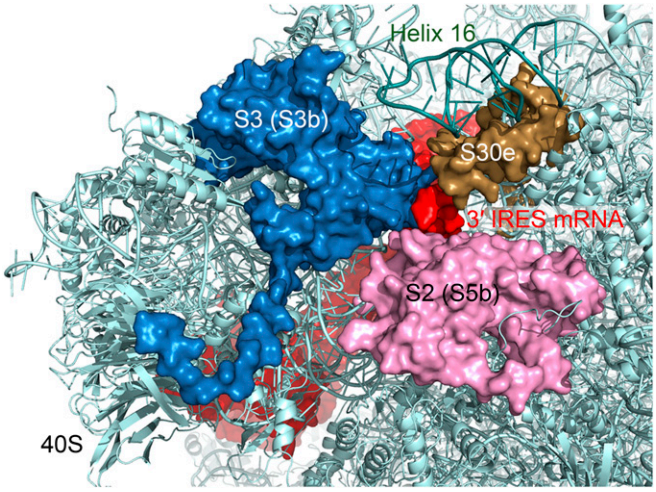

Fig. S5. Interactions of the 3′ end of the TSV IRES RNA with the ribosomal components at the mRNA entrance tunnel in the 40S subunit. Ribosomal proteins S2, S3, and S30e, which interact with the IRES RNA (red), are shown in pink, blue, and brown, respectively. Names of bacterial homologs of S2 and S3 are specified in parentheses. Other small-subunit ribosomal proteins and 18S rRNA are shown in cyan. Helix 16 is highlighted in teal.

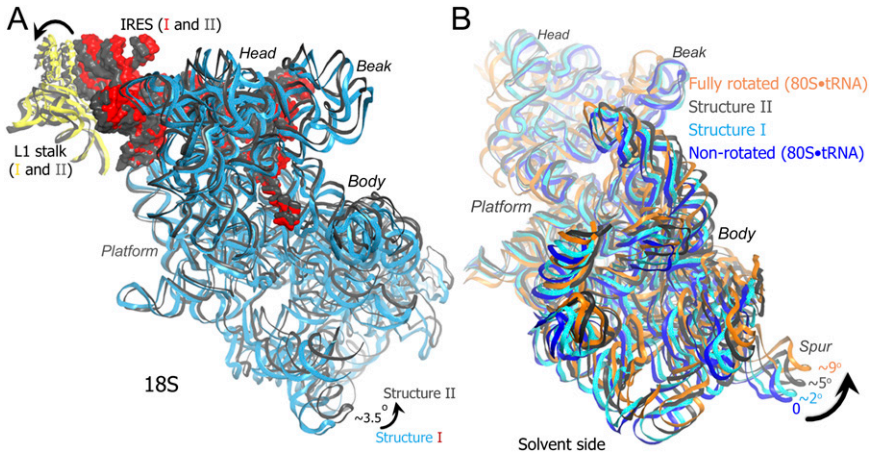

Fig. S6. Conformational differences between the two classes of the 80S•TSV IRES complex (structure I and structure II). (*A*) Rotation of the small 40S subunit in structure II (gray) relative to that in structure I (cyan) is coupled with rotation of the IRES (gray surface in structure II and red surface in structure I) and the L1 stalk of the large subunit (gray ribbon in structure II and yellow ribbon in structure I). The superposition was obtained by structural alignment of the 25S rRNA from the 80S•TSV IRES structure corresponding to structure I on that for structure II. The 40S subunit proteins are not shown for the sake of clarity. (*B*) Comparison of the two conformations of the 40S subunit in the 80S•TSV IRES complex (structure I in cyan and structure II in gray) with the positions of the 40S subunit observed in the fully rotated (orange) and nonrotated (dark blue) 80S•tRNA complexes. The superposition was obtained by aligning 25S rRNAs from the 80S ribosome structures fitted subunit-wise into the corresponding cryo-EM maps [this work (EMDB ID code EMD-5942 and EMD-5943), EMD-5327 (11), and EMD-5329 (11)]. The 40S subunit proteins are not shown for the sake of clarity.

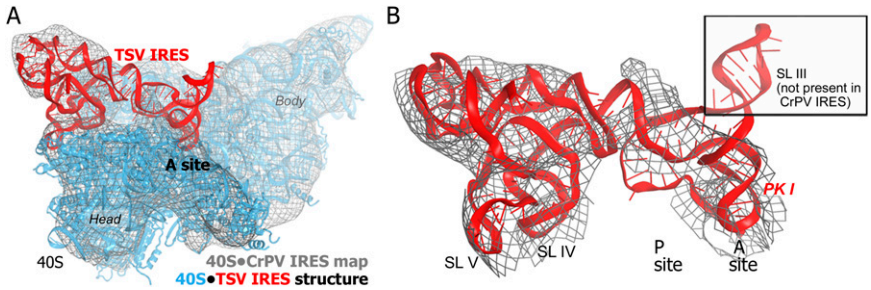

Fig. S7. Comparison of the 80S•IGR IRES and the 40S•IGR IRES complexes. (*A*) Fit of the fragment of the refined 80S•TSV IRES structure (this work), comprising the 40S subunit (cyan) and the IRES RNA (red) into the 20-Å cryo-EM map obtained for the human 40S•CrPV IRES complex (gray; EMD-1090) (52). (*B*) Close-up view of the fit of the TSV IRES (this work) into the 20-Å cryo-EM map obtained for the 40S•CrPV IRES complex (gray), demonstrating that the TSV and CrPV IRESs occupy the same binding site on the small subunit in the context of the 40S (52) and 80S (this work) initiation complexes.

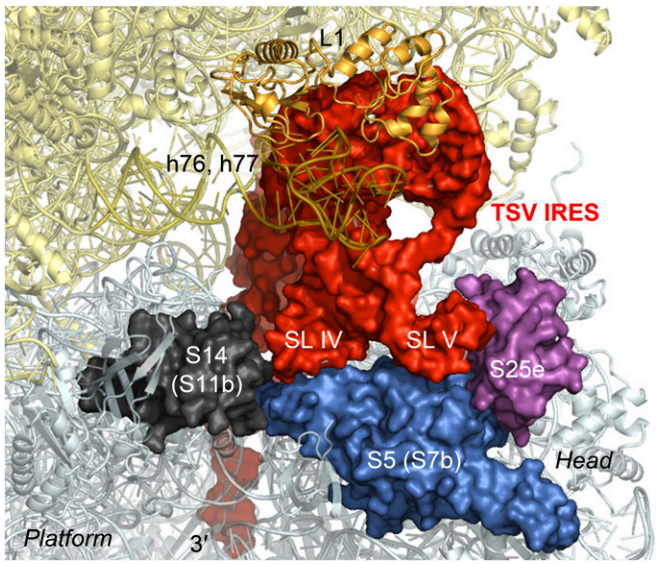

Fig. S8. Interactions of SLIV and SLV of the TSV IRES RNA with ribosomal proteins at the interface between the head and platform of the small ribosomal subunit. SLIV and SLV of the TSV IRES RNA (red surface) bind in a cleft composed of ribosomal proteins S14 (gray), S5 (blue), and eukaryote-specific S25e (purple). Names of bacterial homologs of S5 and S14 are specified in parentheses. The L1 stalk, which interacts with L1.1 of the IRES, is highlighted in orange (L1 protein) and yellow (helices 76 and 77 of 25S ribosomal RNA). For reference, ribosomal RNA and proteins of the large 60S subunit are shown in pale yellow and the small 40S subunit is shown in pale cyan. The view is in the direction from the L1 stalk and E-site region (front view) toward the A site, near which the 3′ end of the IRES-containing mRNA is shown.